ACS OMEGA

Open Access

http://pubs.acs.org/journal/acsodf

Article

Study of Chemical Polymerization of Polypyrrole with SDS Soft Template: Physical, Chemical, and Electrical Properties

Thaneeya Samwang,* Nozomi Morishita Watanabe, Yukihiro Okamoto, Sira Srinives, and Hiroshi Umakoshi*

Cite This: *ACS Omega* 2023, 8, 48946−48957

Read Online

ACCESS | Metrics & More | Article Recommendations | Supporting Information

ABSTRACT: Polypyrrole (PPy) is a conductive polymer known for its biocompatibility and ease of synthesis. Chemically polymerized PPy was synthesized in the presence of sodium dodecyl sulfate (SDS), showing correlations among chemical properties, physical morphology, and electrical properties. Focused synthesis parameters included the pyrrole (Py) concentration, SDS concentration, and ammonium persulfate (APS)/Py ratio. The addition of SDS during chemical polymerization influenced the physical morphology of PPy by altering the self-assembling process via micelle formation, yielding sheet-like morphologies. However, the phenomenon also relied heavily on other synthesis parameters. Varying SDS concentrations within the 0.01 to 0.30 M window produced PPy sheets with no significant difference in optical band gap or physical size. While using 0.10 M SDS, an increase in Py concentration from 0.10 to 0.30 M yielded a larger size of PPy as the morphology changed from sheet-like to irregular shape. The band gap dropped from 2.35 to 1.10 eV, and the conductivity rose from 6.80×10^{-1} to 9.40×10^{-1} S/m. With an increase in the APS/Py ratio, the PPy product changed from a random to a sheet-like form. The product provided a larger average size, a decreased band gap, and increased electrical conductivity. Py polymerization in the absence of SDS revealed no significant change in shape or size as the Py concentration increased from 0.10 to 0.30 M; only a sphere-like form was observed, with a large band gap and small conductivity. Results from Raman spectral analysis indicated a correlation between optical band gap, physical morphology, and bipolaron/polaron ratio, mainly at the wavelengths associated with C−C stretching and C−H deformation. The increase in average size was associated with a decrease in band gap and resistance as well as an increase in the bipolaron/polaron ratio. This work indicates a strong correlation between size, morphology, electrical properties, and the bipolaron/polaron ratio of PPy in the presence of SDS.

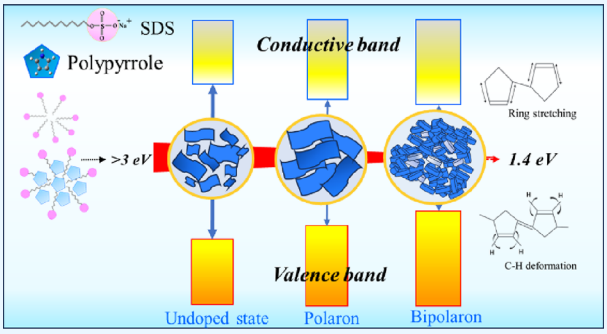

1. INTRODUCTION

Conductive polymers are a group of conjugated polymers that have the ability to incorporate counterions and become semiconductive material. They are flexible, lightweight, and easy to process, similar to a polymer. They enable charge transfer and offer moderate conductivity, akin to that of semiconductors. These outstanding properties of conductive polymers make them promising candidates for various applications, including sensor devices,[1−5] surface coatings, electronic circuits, energy storage devices,[6−8] and medical equipment.[9−11] Examples of conductive polymers are polythiophene, polyaniline, and polypyrrole (PPy). PPy has gained considerable attention from researchers worldwide because of its high conductivity, thermal stability, and biocompatibility.[12,13]

The electrical conductivity of a semiconductor correlates with its optical band gap, which is the difference between the energy levels of its valence and conductive bands. The optical band gap of a semiconductor is one of its crucial properties that indicate the mobility of the charge carriers in the semiconductor and the activities involved in the reactions and interactions within it.[14,15] PPy offers band gaps of 1 and 3 eV,[16,17] depending on its pre- and postsynthesis parameters in the polymerization process, such as the type of counterions, degree of doping, and oxidation state.[18−21] Chemical polymerization is a simple method of synthesizing PPy via an oxidation−reduction reaction and applying it to industrial-scale production. This method required oxidizing agents, such as ferric chloride or ammonium persulfate, to oxidize the pyrrole monomer (Py), initiating the polymerization process. The oxidized Py reacts with the remaining Py or other oxidized Py to form dimers, trimers, and oligomers.[22,23] The oligomers produce nuclei and PPy. The degree of oxidation of PPy is

Received: August 30, 2023
Revised: November 8, 2023
Accepted: November 23, 2023
Published: December 13, 2023

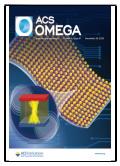

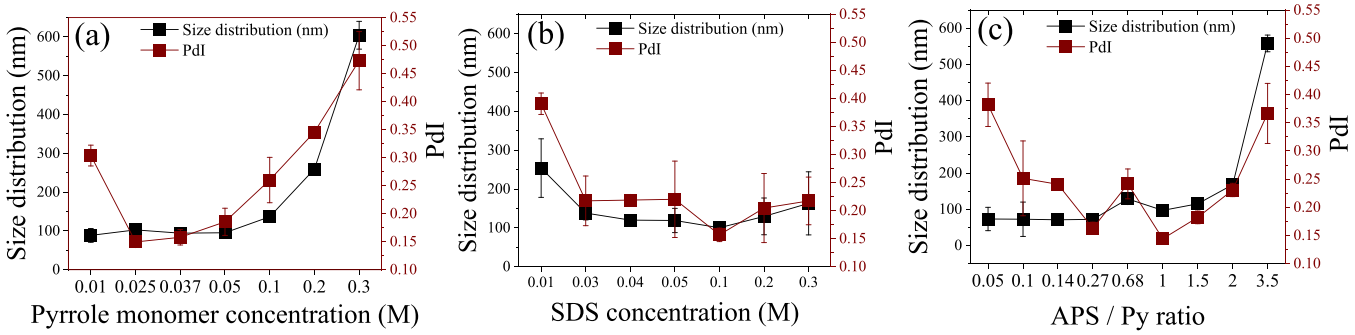

Figure 1. Average size distribution and PdI of PPy synthesized using (a) varied Py monomer concentrations at 0.10 M SDS and an APS/Py ratio of 1.00, (b) varied SDS concentrations, 0.04 M Py, and an APS/Py ratio of 1.00, and (c) varied APS concentrations (represented by varying APS/Py molar ratio), 0.10 M SDS, and 0.04 M Py.

associated with the presence of polaron- and bipolaron-localized lattice distortion defects in polymeric structure that drive charge carrier mobility,[24,25] in which polarons and bipolarons represent a low and high oxidative states, respectively.[26−28] The formation of polarons and bipolarons depends heavily on synthesis conditions and contributes to the morphology and chemical and electrical properties of the PPy. Santos et al.[28] and Pang[29] studied chemical polymerization of PPy relying on Raman spectroscopy analysis. They reported that Py rings preferentially bind at the alpha−alpha ($\alpha-\alpha$) positions but can connect at the beta−β ($\beta-\beta$) and beta−α ($\beta-\alpha$) positions. The binding positions affect molecular structures of dimers and trimers as well as their oxidative states, which are represented in terms of bipolarons and polarons of the PPy. Ishpal and Kaur, Bober et al., Trchová and Stejskal, and Šetka et al.[30−33] synthesized the different PPy nanostructures, such as nanorods, nanoparticles, and nanospheres, based on chemical polymerizations. Raman spectra showed that peak spectra of bipolarons and polarons were associated with synthesis conditions and were correlated with morphological, chemical, and electrical properties of the PPy.

Template-assisted polymerization is a well-known technique that utilizes soft or hard templates to form a certain physical morphology of a polymer. The technique was demonstrated in a synthesis of various PPy nanostructures, including nanospheres,[34,35] nanotubes or nanowires,[36−38] nanorings,[39] and nanosheets.[40−42] In a hard template technique, a solid mold was applied for polymerization, providing the physical morphology that the polymer grew in and subsequently adopted. The soft template, on the other hand, exercised the concept of self-assembly polymerization, relying on a unique reaction or interaction between a monomer and a soft template substance in attaining a designed physical morphology. Sodium dodecyl sulfate (SDS) is an anionic surfactant that has been widely studied for its ability as a soft template. Utilization of SDS in a soft template polymerization of PPy yielded icosahedrons[43] and spherical,[44−46] cylindrical, and elongated structures[44,46] and was also reported to promote electrical conductivity.[43,47] Regardless of the popularity of the SDS, the mechanisms underlying the correlation between physical, chemical, and electrical conductivity are not fully understood. A study of the use of SDS-assisted chemical polymerization for PPy synthesis can deepen our understanding of the molecular-level phenomena and affect the other properties of PPy.

This study aimed to (1) investigate the effects of SDS on the chemical polymerization of PPy and (2) explore the correlations among PPy properties, focusing on size, morphology, optical band gap, resistance, and bipolaron/polaron ratios. Py was polymerized in the presence of SDS with ammonium persulfate (APS) as an oxidizer. Synthesis parameters, including SDS concentration, Py concentration, and APS/Py ratio, were varied and studied.

2. RESULTS AND DISCUSSION

2.1. Physical Characterizations. PPy samples were synthesized in the presence of SDS, which served both as a surfactant and as a counterion. As a surfactant, SDS interacts with Py and other radicals in polymerization solutions and determines the physical shape of the PPy. As a counterion, SDS incorporates a negative polar on the polymeric chain, promoting a degree of oxidation for PPy. In the first operation, PPy was synthesized with varied Py concentrations (0.01−0.30 M) and a constant SDS concentration (0.10 M). Dynamic light scattering (DLS) analysis revealed that the average particle size of PPy ranged from 88.40 to 94.20 nm for a Py concentration of 0.01 to 0.04 M. The polydispersity index (PdI) is defined by Malvern Panalytical Co., Ltd., as a calculated dimensionless number (Figure 1), showing dispersibility between 0.05 (mono disperse) and 0.70 (broad size distribution). At 0.01−0.04 M Py, the PdI decrement suggested a higher degree of uniform distribution in PPy chain length for increased Py concentration. An increase in Py concentration from 0.04 to 0.30 M raised the particle size from 94.20 to 604.50 nm and PdI values from 0.15 to 0.47, which indicated a higher chain length distribution. In the second operation, the effects of SDS concentration (0.01 to 0.30 M) on PPy formation at constant Py concentration (0.04 M) were studied. The selected range of SDS concentration exceeded the critical micelle concentration (CMC) of 0.008 M,[38,39] signaling that SDS micelles were formed. As the SDS concentration increased from 0.01 to 0.10 M, the average particle size of PPy dropped from 253.90 to 100.10 nm, corresponding to PdI values of 0.39 and 0.16. The results agree with those of previous studies,[24,30,40] showing a reduction in particle size with increasing surfactant concentration. As the SDS concentration increased from 0.10 to 0.30 M (Figure 1b), the particle size increased from 100.10 to 163.10 nm and the PdI increased from 0.16 to 0.26. In the third operation, the effect of APS was assessed from the molar ratio of APS/Py. When the APS/Py ratio increased from 0.10 to 3.50, the particle size of PPy increased from 73.50 (PdI = 0.25) to 557.90 nm (PdI = 0.37; Figure 1c). APS in the mixture served as an oxidizing agent that reacted directly with the Py monomer, initiating the chemical polymerization. As the APS/Py ratio increased, the polymerization rate rose,

https://doi.org/10.1021/acsomega.3c06511
ACS Omega 2023, 8, 48946−48957

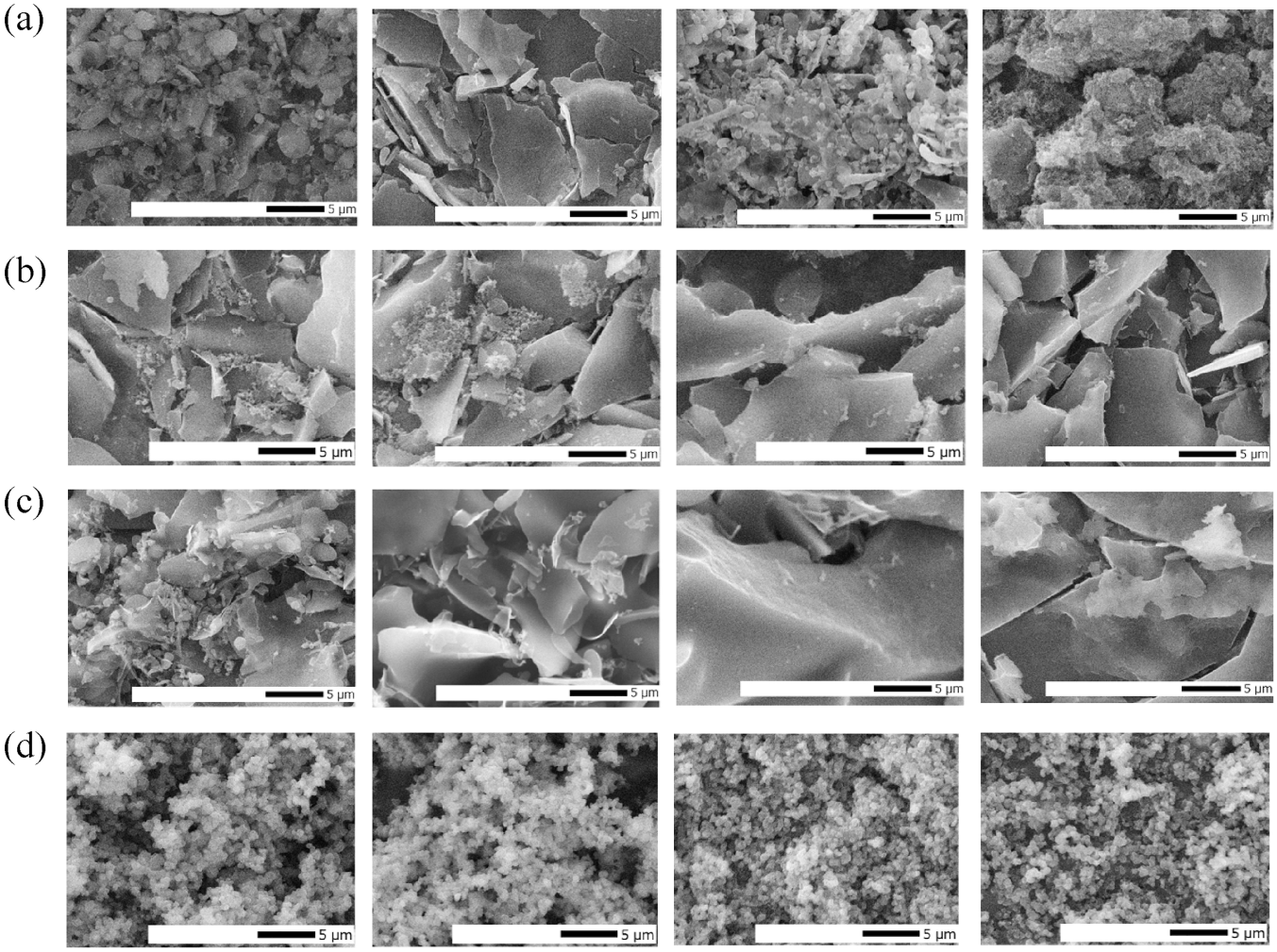

Figure 2. SEM images (×5000) of PPy synthesized using (a) Py concentrations of 0.01, 0.04, 0.10, and 0.30 at 0.1 M SDS and APS/Py = 1.00 (left to right). (b) SDS concentrations of 0.01, 0.04, 0.10, and 0.30 at 0.04 M Py and APS/Py = 1.00. (c) APS/Py ratios of 0.27, 0.68, 1.5, and 3.5 at 0.1 M SDS and 0.04 M Py. (d) Py concentrations of 0.01, 0.04, 0.10, and 0.30 M with no SDS and APS/Py = 1.00.

Scheme 1. Diagrams Showing PPy Morphologies for Different Py, SDS, and APS Concentrations: A = Random Form, B = Sheet-Like Form, C = Flake-Like Form, D = Irregular Form, and E = Sphere-Like Form

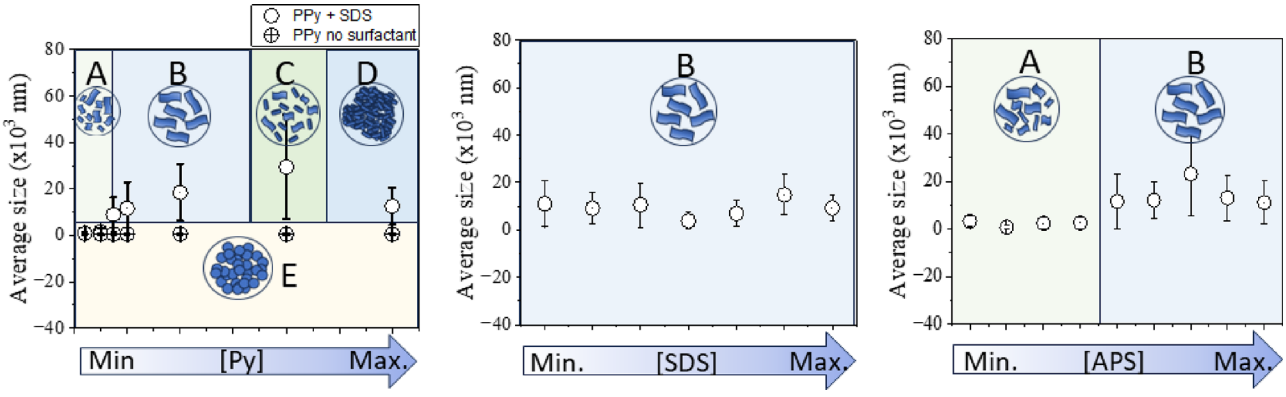

yielding increased particle size. The results provide strong evidence of the direct correlation between the PPy particle size and PdI values.

Scanning electron microscopy (SEM) was used to analyze the physical morphology of the PPy samples (Figure 2). The SEM images showed that PPy had a variety of shapes and that it firmly relies on the synthesis parameters, namely, Py concentration, SDS concentration, and APS/Py ratio.[41] The particle size was determined from images using the ImageJ program (ImageJ Version 1.53 K, National Institutes of Health, USA). Figure 2a shows the SEM images of PPy samples from the first operation, with Py concentrations varying from 0.01 (left) to 0.04, 0.20, and 0.30 M (right). For 0.01 M Py, the PPy sample was a combination of sheets and particles, with an

https://doi.org/10.1021/acsomega.3c06511
ACS Omega 2023, 8, 48946−48957

average size of 0.94 μm. For 0.04 M Py, PPy became a sheet-like structure with an average length of 8.93 μm. As the Py concentration increased from 0.20 to 0.30 M, PPy aggregated and acquired an irregular shape with average particle sizes of 33.77 and 12.55 μm, respectively (Scheme 1). SEM images of PPy samples from the second operation (Figure 2b) provided information about SDS concentration effects on the physical morphology of PPy. The PPy sheets appeared smaller, changing from 11.01 to 6.93 μm, as the SDS concentration increased from 0.01 to 0.10 M. The increase in SDS concentration to 0.20 and 0.30 M enlarged the size of the PPy sheets into 14.81 and 9.27 μm. PPy samples from the third operation revealed that variations in the APS/Py ratio led to different polymerization rates and physical structures (Figure 2c). As the ratio increased from 0.27 to 0.68, the PPy shape changed from a combination of particle and sheet shapes (3.17 μm) to a sheet-like form (11.62 μm). The sheets grew to 21.76 and 12.86 μm, corresponding with the ratios of 1.50 and 3.50. A set of control experiments was studied by performing chemical polymerization in the absence of SDS (Figure 2d) and varying the concentration of Py from 0.01 to 0.04, 0.10, and 0.30 (APS/Py ratio 1:1). PPy samples assigned as PPy* (PPy synthesized in the absence of SDS) exhibited particle morphology with average sizes of 646 (left), 614, 718, and 667 nm (right), respectively.

During chemical polymerization, SDS was a bifunctional substance, acting as a soft template in forming PPy sheets and doping PPy for enhanced electrical conductivity.[38,39] In its soft template role, SDS established micelles at a concentration higher than its CMC of 0.008 M. The micelles became compact when the SDS concentration increased, yielding micellar lamellae or hexagons at an extra-high SDS concentration.[42,48] In the presence of water, the SDS molecules turn their hydrophilic parts toward water, hiding hydrophobic branches inside the micelles. The Py monomer is a hydrophobic substance (Log P = 0.75, where P is the partition coefficient between octanol and water), and it could be surrounded by SDS, allowing the hydrogen in the Py to interact with the hydrophobic branches in SDS. The interactions result in a Py distribution and particle formation at the micelle centers. The zeta potentials of PPy and PPy* were monitored using DLS, and their observed values were in the ranges of −32 to −20 mV and from 20 to 25 mV, respectively. The potential suggested that chemical polymerization had occurred and that PPy had been formed within the micelles. The polymerized PPy was encapsulated by SDS, which prevented it from aggregating with other particles. The phenomenon resulted in the dispersion of PPy colloids and the formation of a sheet-like PPy structure. Such phenomena, however, were limited to synthesis conditions in which the amounts of Py, SDS, and APS were balanced. Figure 2a shows, at a low Py concentration of 0.01 M, PPy consisting of particles and a sheet-like form. As the Py concentration increased from 0.04 to 0.10 M, a sheet-like PPy structure was formed. At a Py concentration of 0.20 and 0.30 M, PPy overgrew to create an irregular structure.

The effect of the SDS concentration on PPy growth was studied next (Figure 2b). The sheet-like PPy structure increased in size as the SDS concentration increased from 0.01 to 0.04, and 0.10 M and appeared to be constant as the SDS concentration of 0.30 M was realized. Figure 2c presents the effects of the APS/Py ratio on the PPy morphology. PPy was polymerized at varied APS/Py ratios, 0.10 M SDS, and 0.04 M Py. The APS/Py ratio of 0.27 yielded a combination of PPy particles and sheets, while the ratios of 0.68, 1.50, and 3.50 revealed large PPy sheets. The effects of SDS on PPy formation are summarized in Scheme 2. SDS micelles were loosely

Scheme 2. Diagrams Proposing Mechanisms for PPy Formations Synthesized in the Solutions with (a) SDS, (b) Py and SDS, (c) Py, SDS, and APS, and (d) PPy with a APS/Py Ratio of 1.00 after 24 h; SEM Images Showing PPy Samples at ×5000 Magnification (Freeze-Dried Powder)

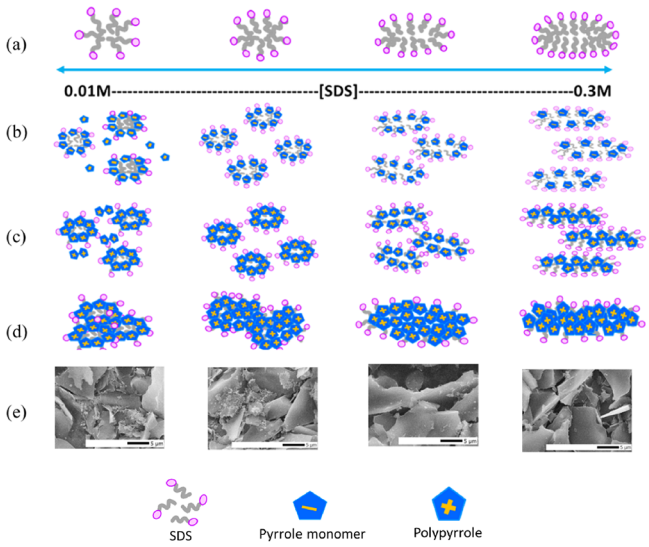

assembled at a low SDS concentration (0.01 M), fully assembled at a moderate SDS concentration (0.04 M), and expanded at high SDS concentrations (0.20−0.30 M) (Scheme 2a). Py interacted with and was encapsulated within the micelles (Scheme 2b). As Py reacted with APS, polymerization occurred (Scheme 2c) and the growth continued inside the micelles (Scheme 2d). Py polymerized in SDS micelles and formed a sheet-like structure.

2.2. UV−vis-NIR Absorbance of PPy and Its Optical Band Gap Determination. The light absorbance of PPy samples was analyzed using UV−vis-NIR spectroscopy, and the optical band gap of the samples was determined. The absorption spectra of PPy were monitored in the 200−1000 nm wavelength window. Two absorption peaks were observed: one between 428 and 475 nm and the other between 835 and 930 nm (Figure 3a−c). The first peak (428−475 nm) corresponds to a $\pi-\pi^*$ transition, suggesting the presence of neutral and polarons in PPy.[17,49] The second peak (820−930 nm) corresponds to the oxidized bipolarons of the PPy chain.[27,50] In Figure 3a, the PPy obtained using 0.01 and 0.03 M Py shows negligible absorbance at the neutral polarons and oxidative bipolaron spots but shows peaks at wavelengths of 297 and 284 nm. These peaks can be ascribed to the SDS signals (Figure S3), indicating the SDS incorporation into PPy samples. The PPy samples synthesized at 0.04 M Py showed light absorption peaks at 448 and 841 nm, which correlated with polarons and bipolarons, respectively. When the Py concentration increased from 0.04 to 0.30 M, the two light absorption peaks shifted from 448 to 475 nm and from 841 nm to a longer wavelength (outside the measurement range). The shifts indicated a higher degree of Py oxidation at high Py concentrations,[17,51] suggesting that a larger-sized PPy was produced for a more concentrated Py solution (Figure 1a).

https://doi.org/10.1021/acsomega.3c06511
ACS Omega 2023, 8, 48946−48957

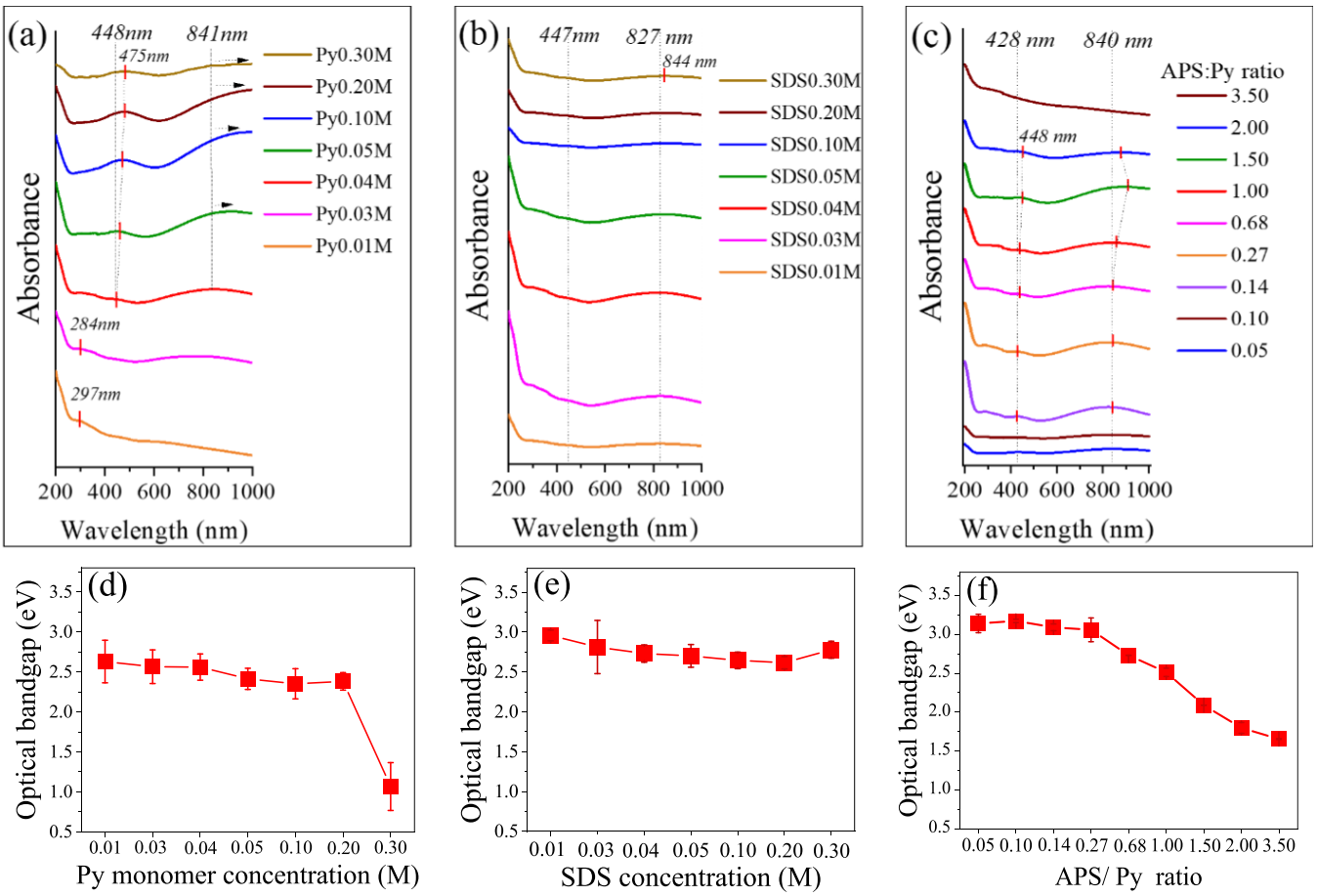

Figure 3. Light absorbances of PPy samples synthesized from a solution with (a) varied Py concentrations (0.10 M SDS and APS/Py = 1.00), (b) varied SDS concentrations (0.04 M Py and APS/Py = 1.00), and (c) varied APS/Py ratio (0.10 M SDS, 0.04 M Py). The optical band gap of PPy changing with (d) increased Py concentration, (e) increased SDS concentration, and (f) increased APS/Py ratio.

The increased oxidation degree was also associated with PPy shape transformation from a combination of particles and sheet-like structures to sheet-like structures and irregular shape (0.30 M Py) (Figure 2a). These can be attributed to a limited number of SDS micelles at elevated Py concentrations, which lowers their effectiveness in facilitating the growth of PPy sheets.

When the SDS concentration was varied while the Py concentration was maintained at 0.04 M, the absorbance peaks of PPy remained more stable than they were during the variation of Py concentration. An increase in SDS concentration from 0.01 to 0.30 M caused a negligible change in the position of the neutral polaron peak at 447 nm, and a slight shift in the bipolaron peak from 827 to 844 nm (Figure 3b). The results support that SDS has a dual function: (i) as a surfactant in polymerization and (ii) as counterions of PPy. The shift in bipolaron peak can be attributed to the partial doping of PPy with SDS.

When the APS/Py ratio increased from 0.14 to 0.27, the absorbance peaks of the polarons and bipolarons shifted from 428 to 431 nm and from 840 to 835 nm, respectively. As the ratio increased to 0.68, 1.00, and 1.50, the neutral polaron peak shifted from 438 to 442 and 448 nm whereas the oxidative bipolaron peak shifted from 840 to 842 and 894 nm. As the APS/Py ratio increased from 1.50 to 2.00, the bipolaron peak shifted from 894 to 843 nm while the polaron peak remained at 448 nm. At an APS/Py ratio of 3.50, the bipolaron peak disappeared completely. An increase in the APS/Py ratio provides Py with more oxidizing agents, enhancing the growth and oxidative levels of PPy. On the other hand, a high APS content can overoxidize PPy, preventing it from growing further.[52,53] Thus, the sheet-like structures were formed even at a relatively high APS/Py ratio.

The optical band gap of PPy samples was determined based on the light absorption data from the UV−vis-NIR and Tauc's correlation (Figure 3d−f and Figure S4). The band gap of PPy continued to decrease as the Py concentration increased at a constant SDS concentration and APS/Py ratio. As the Py concentration increased from 0.01 to 0.20 M, the optical band gap decreased from 2.63 to 2.38 eV. A significant decrease in the band gap to 1.10 eV occurred when the Py concentration reached 0.30 M (Figure 3d). A reduction in the band gap implies that the energy required for an electron to travel from the valence band to the conductive band is reduced, indicating that the PPy synthesized at a high Py concentration has a high electrical conductivity. These results agree well with the results from the SEM analysis, which shows that morphology changes from particles to sheets, and irregular structures correspond to the increase in the Py concentration. The degree of oxidation of PPy was enhanced for the increased surface area. An increase in SDS concentration from 0.01 to 0.30 M, at the constant Py concentration and APS/Py ratio, caused a slight reduction in the PPy band gap, reducing from 2.96 to 2.78 eV (Figure 3e).[44] The variation of the SDS concentration during

https://doi.org/10.1021/acsomega.3c06511
ACS Omega 2023, 8, 48946−48957

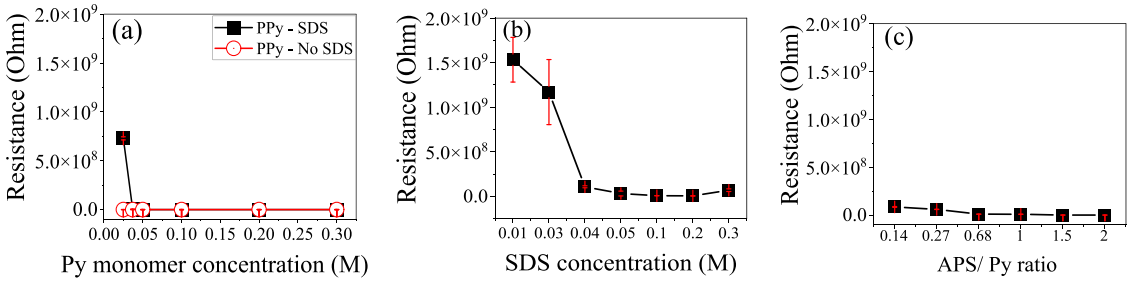

Figure 4. Resistance of PPy polymerized by varying (a) the Py concentration (0.10 M SDS and APS/Py = 1.00), (b) the SDS concentration (0.04 M Py and APS/Py = 1.00), and (c) the APS/Py ratio (0.10 M SDS and 0.04 M Py).

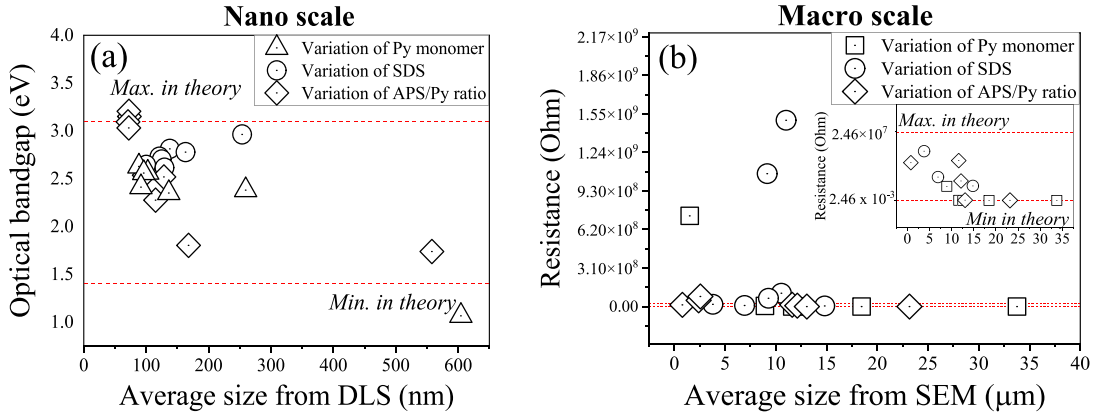

Figure 5. Correlation between the (a) optical band gap and average particle size of PPy and (b) resistance and average particle size of PPy as observed from SEM images.

the synthesis of PPy did not result in a significant difference in the band gap.

Throughout the alteration of the APS/Py ratio, with constant SDS and Py concentrations, the ratio increments from 0.10 to 0.27 yielded negligible alterations in the optical band gap, ranging from 3.21 to 3.03 eV. As the ratio increased from 0.68 to 3.50, the band gap of PPy decreased from 2.52 to 1.74 eV (Figure 3f). It is worth noting that as the APS/Py ratio varied from 0.01 to 3.50, the PPy shape transformed from particles to a sheet-like structure, which can contribute to the band gap reduction of PPy.

2.3. Electrical Conductivity of PPy Films. PPy and PPy* samples were fabricated to a chemiresistive device (Scheme S1), in which the polymer film was sandwiched by the ITO electrodes, and the electrical conductivity was monitored. The device was analyzed in a linear sweep voltammetry (LSV) mode at a scan range of ±1.8 V and a scan rate of 50 mV/s to obtain the resistance and conductivity, respectively. The resistance of the PPy sample device decreased from 0.73 GΩ to 43.58 Ω for the PPy from Py concentrations of 0.03 and 0.30 M (Figure 4a). The resistance of the PPy* device reduced from 28.04 kΩ to 397.70 Ω for the PPy* synthesized from 0.03 and 0.30 M Py with no SDS (Figure 4a). These results support our finding that utilization of SDS, with proper amounts of Py and APS, in the chemical polymerization of PPy can effectively enhance PPy conductivity.[52,54] The resistance of PPy decreased from 1.50 GΩ to 5.29 MΩ when the SDS concentration increased from 0.01 to 0.20 M (Figure 4b). In this study, we observed a substantial alteration in the PPy resistance when the SDS concentration was at or below 0.04 M, which is close to the CMC values (0.008 to 0.0083 M).[38,39] When the SDS content was low, PPy acquired irregular shapes (correlating with a high PdI, 0.39), yielding poor adhesion and electrical contacts between each PPy particle. The phenomenon led to a high resistance for the PPy chemiresistive device.[43] When the APS/Py ratio increased from 0.14 to 2.00 (constant SDS and Py concentration), the device resistance decreased from 50.19 MΩ to 80.32 kΩ (Figure 4c). The correlation between the resistance of PPy and its band gap is depicted in Figure 3d−f, stating that a decrease in the band gap leads to a reduction resistance. As the APS/Py ratio increased from 0.68 to 2.00, the resistance of PPy decreased from 15.00 MΩ to 80.32 kΩ, the band gap decreased from 2.52 to 1.80 eV, and the morphology was presented in sheet-like form.

The reduction in resistance and band gap partly corresponds to the morphology change from a random to a sheet-like form. The results are summarized in Figure 5a, showing that the band gap of PPy is in the range of 3.16 to 1.46 eV and that PPy changed from an undoped state to an oxidized and fully doped state.[15,27,54] Figure 5a displays this as the size of the PPy particles increased from 50 to 600 nm and the band gap decreased. This observation is consistent with the behavior observed in silicon or gallium phosphide or indium arsenide.[55] We observed that the band gap of PPy tended to cluster at approximately 2.50 eV, which agrees well with the results obtained in a previous study.[44,56] The PPy band gap obtained using UV−vis-NIR revealed that the polymerization oxidized PPy but could not fully transform it into a doped state except at a Py concentration of 0.30 M. This limitation resulted in a band gap of 1.10 eV and an average particle size of 604.50 nm.

The electrical resistances of PPy samples are summarized in Figure 5b, showing the resistances in the reference range of 2.46×10^{-3} to 2.46×10^{7} Ω.[57] The resistance was calculated from resistivity using eqs 2 and 3. Figure 5b shows that the

https://doi.org/10.1021/acsomega.3c06511
ACS Omega 2023, 8, 48946−48957

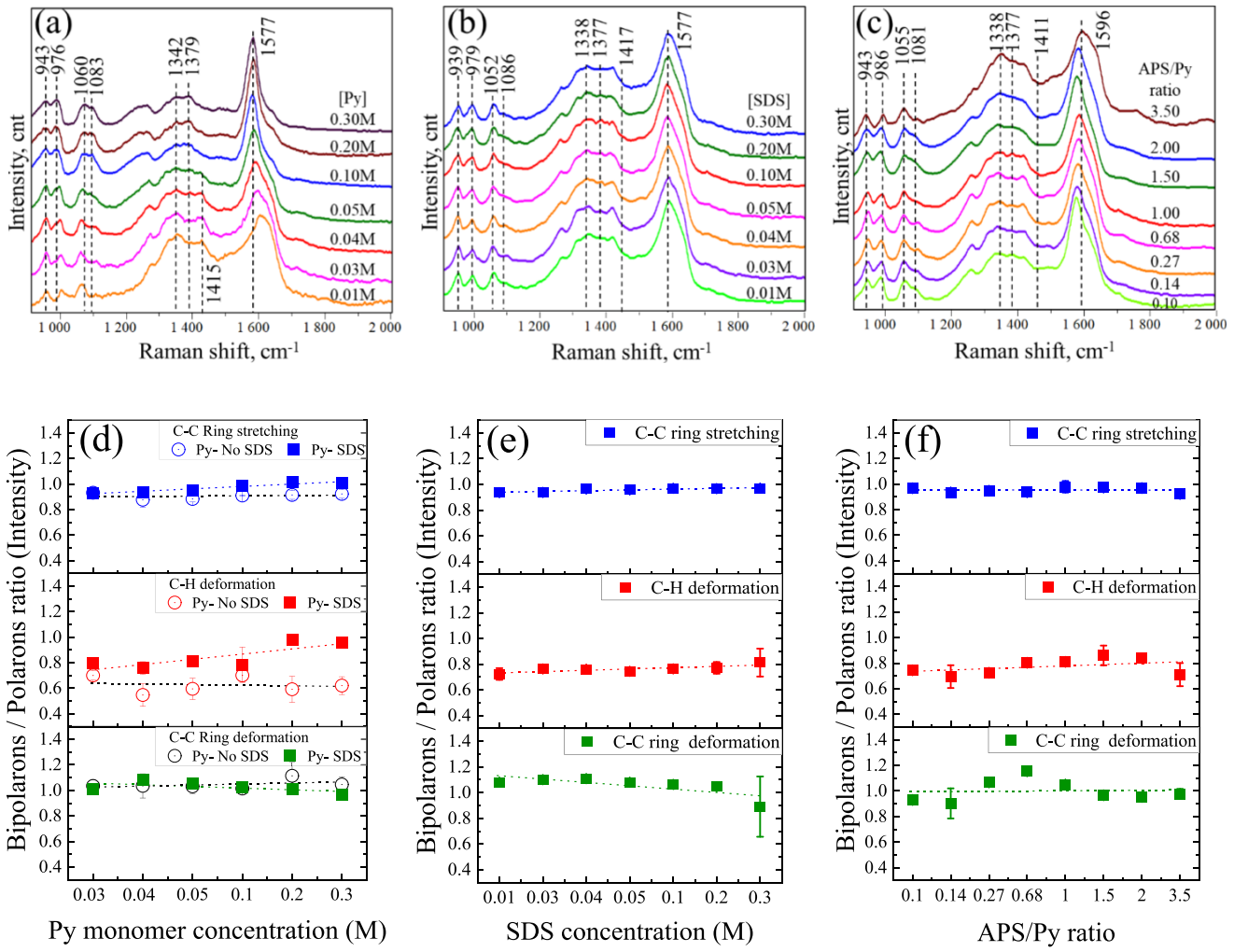

Figure 6. Raman spectra of PPy synthesized by varying the (a) Py concentration, (b) SDS concentration, and (c) APS/Py ratio. The bipolaron-to-polaron ratio of the PPy synthesized by varying the (d) Py concentration (at 0.10 M SDS and an APS/Py = 1.00), (e) SDS concentration (at 0.04 M Py and an APS/Py = 1.00), and (f) APS/Py ratio (at 0.10 M SDS and 0.04 M Py).

resistance of PPy decreases as its particle size increases, which is consistent with Figure 5a. At low Py concentrations of 0.01 and 0.03 M, SDS concentrations of 0.01, 0.03, 0.04, and 0.30 M, and low APS/Py ratios of 0.10, 0.14, and 0.27, the resistance was higher than that in the reference range. This can be addressed since PPy provided smaller size particles, sheets, or flake structures in those synthesis conditions, and the electrical resistance was monitored from the chemiresistive device. The resistance obtained from the device was a combination of intrinsic and extrinsic resistances,[58] where the former and the latter were correlated with PPy conductivity and contacts between PPy samples, respectively. In the case of smaller PPy particles, a high number of contacts occurred, leading to the domination of contact resistance instead of material resistance. This assumption also explained high electrical resistance in the case of an irregularly shaped PPy, which followed the extrinsic resistance-dominating model. At a high SDS concentration of 0.30 M, PPy has a sheet-like structure with a high resistance of 67.00 MΩ, indicating that a too high SDS concentration can disturb the conductivity of PPy.

2.4. Bipolaron and Polaron Structures of PPy and Its Electronic Properties. Raman spectroscopy was used to analyze the chemical functionalities of PPy. The PPy sample was excited at 532 nm, yielding signals for polarons and bipolarons (Table S1).[33,49] The Raman spectra shown in Figure 6a–c indicate similarities in peaks, including C−C ring deformation for bipolarons (926−927 cm^{-1}) and polarons (963−985 cm^{-1}), C−H deformation for polarons (1050−1056 cm^{-1}) and bipolarons (1079−1084 cm^{-1}), and C−C ring stretching for the polarons (1330−1344 cm^{-1}) and bipolarons (1377−1382 cm^{-1}). The C═C stretching peak appeared at 1562−1593 cm^{-1} for the polarons but was not detected at 1600 and 1618 cm^{-1} for the bipolarons.

In Figure 6a, when the Py concentration increased from 0.01 to 0.30 M while the SDS concentration and APS/Py ratio remained unchanged, the polaron peak corresponding to C−C ring deformation shifted from 986 to 976 cm^{-1}. The C−C ring deformation of the bipolarons (926−927 cm^{-1}) remained almost unchanged. The polaron peak that shifted to the left supported a highly oxidized chain of PPy.[32] As the Py concentration increased, the C−H deformation peak associated with the polarons shifted from 1050 to 1060 cm^{-1}. This shift indicated an increase in the oxidative degree of PPy.[32] Additionally, with an increased Py concentration, a C−H deformation peak of the bipolarons emerged and was enhanced at 1083 cm^{-1}. The C−C ring stretching remained constant for the polarons (1340−1342 cm^{-1}) and moved to the left (from

https://doi.org/10.1021/acsomega.3c06511
ACS Omega 2023, 8, 48946−48957

1387 to 1379 cm^{-1}) in the case of the bipolarons. The peak shift from 1415 to 1410 cm^{-1} can be attributed to the C−C and C−N stretching of oxidized PPy in the ring structure.[25,49,53] This shift was observed as the Py concentration increased from 0.01 to 0.05 M and was difficult to follow at Py concentrations exceeding 0.05 M. The shift toward a lower frequency range indicates the transition of PPy to a neutral state during its C−N stretching.[33] The C═C stretching peak of the polarons shifted from 1599 to 1579 cm^{-1} as the Py concentration increased from 0.01 to 0.30 M. The shift toward a smaller wavenumber indicated switching from an oxidative to a neutral state,[43,59] while a narrow and sharp C−C peak corresponded to a high degree of crystallinity.[60]

As the SDS concentration varied from 0.01 to 0.30 M during PPy synthesis (constant Py concentration and APS/Py ratio), the C−C peak did not shift (Figure 6b). The C−C ring deformation of bipolarons (939 cm^{-1}) and polarons (979 cm^{-1}) moved to the left and right, respectively. The C−H deformation showed a similar trend in which the C−H deformation of bipolarons shifted left (1052 cm^{-1}) and polarons shifted right (1086 cm^{-1}). The C−C ring stretching peak for polarons was at 1338 cm^{-1}, while the C−C and C−N stretching peaks for bipolarons were at 1377 and 1417 cm^{-1}, respectively. The SDS concentration did not significantly affect the degree of PPy oxidation, but the presence of SDS promoted PPy oxidation.

An increase in the APS/Py ratio from 0.10 to 3.50 did not shift the C−C ring deformation peak for polarons but provided a slight shift in the C−C ring deformation for bipolarons (946−943 cm^{-1}) (Figure 6c). The C−H deformation peaks remained unchanged, while the APS/Py ratio varied, revealing peaks of polarons and bipolarons at 1055 and 1081 cm^{-1}, respectively. The C−C ring stretching peaks of the polarons and bipolarons remained insensitive to changes in the APS/Py ratio and were present at 1338 and 1377 cm^{-1}. The C−C and C−N stretching peaks of the ring structure appeared at 1411 cm^{-1} unchanged as the ratio changed. The C═C stretching peaks of the polarons appeared at 1596 cm^{-1} when the APS/Py ratio was 3.50 and shifted to the left when the ratio increased from 0.10 to 2.00.

2.5. Bipolaron-to-Polaron Ratio and Electronic Properties and Morphology of PPy. The bipolaron/polaron ratio provided information on the oxidative state of PPy and was obtained by dividing the peak intensity of bipolarons by that of polarons. Our focus was on the analysis of C−C ring deformation, C−H deformation, and C−C ring stretching (Figure S5).

For C−C ring deformation (Figure 6d), the bipolaron/polaron ratio increased from 1.08 to 0.96 as the Py concentration increased from 0.03 to 0.30 M. The corresponding ratio for PPy* remained almost unchanged (1.01 to 1.05) as the Py concentration increased. The bipolaron/polaron ratio with respect to the C−H deformation of PPy increased from 0.76 to 0.94 as the Py concentration increased. The corresponding ratio of PPy* fluctuated between 0.55 and 0.70 irrespective of the Py concentration (0.03 to 0.30 M). SDS promoted the C−H deformation in PPy and affected its physical morphology (Figure 2a−c). The bipolaron/polaron ratio of PPy correlated with its C−C ring stretching, which grew from 0.93 to 1.03 as the Py concentration increased from 0.03 to 0.30 M. The corresponding ratio of PPy* remained almost constant within the range of 0.88−0.93. The increased bipolaron/polaron ratio related to the C−C ring stretching of PPy resulted in the reduction of its band gap from 2.63 to 1.10 eV. As the Py concentration increased from 0.10 to 0.30 M, the bipolaron/polaron ratio of the C−C ring stretching in PPy increased and triggered a decrease in the resistance of PPy (Figure 4) and its band gap (Figure 3). These results suggest that the increased bipolaron/polaron ratio of C−C ring stretching in PPy enhanced its conductivity. These results showed that SDS can modify the oxidative state of PPy. Additionally, the comparison between the morphology and the bipolaron/polaron ratio showed alignment with the transformation of the PPy structure. The morphology of PPy transformed from a random form to a sheet-like structure (Figure 2a) when the Py concentration increased from 0.10 to 0.30 M while using 0.10 M SDS, but the shape of PPy* has a sphere-like form (Figure 2d). From the bipolaron/polaron ratio of PPy and PPy*, we found that the value in the bipolaron/polaron ratio of C−H deformation of PPy is higher than that of PPy* as the Py concentration increased, as mentioned above. It is possible that SDS functions as a dopant and interferes with the formation of the PPy structure during Py polymerization,[17,26] as represented in the C−H deformation of the Raman spectra. The change in C−H deformation affects the gap energy, as shown in the relational tendency with the band gap. That is, the bipolaron/polaron ratio in the C−H deformation of PPy increased from 0.80 to 0.94, resulting in a reduction of its band gap from 2.63 to 1.10 eV (Figure 3d) and its resistance from 0.73 GΩ to 43.58 Ω (Figure 4a) as the Py concentration increased from 0.10 to 0.30 M while using 0.10 M SDS.

In the varied SDS concentration experiment at a constant Py of 0.04 M and an APS/Py ratio of 1, no significant change in the bipolaron/polaron ratio (Figure 6e) was observed since the C−C deformation varied from 1.08 to 0.89, C−H deformation from 0.72 to 0.81, and C−C ring stretching from 0.94 to 0.97. When considering these results together with the analysis from size (ranging from 100.10 to 253.90 nm), band gap (2.62 to 2.96 eV), and shape (as a sheet-like structure), these findings indicate that not much of the electrical and chemical properties of the PPy were altered at various SDS concentrations and that the extrinsic property, contact resistance, was the key to resistance change.

As Figure 6f shows, the bipolaron/polaron ratio of C−C ring deformation first increased from 0.90 to 1.15 and decreased to 0.98 when the APS/Py ratio increased while the Py and SDS concentrations remained constant. The C−H deformation first increased from 0.69 to 0.86 and then decreased to 0.71 as the APS/Py ratio increased. During C−C ring stretching, the bipolaron/polaron ratio first changed slightly from 0.93 to 0.98 and then decreased to 0.92 when the APS/Py increased. These trends correspond to the change in the bipolaron state observed using UV−vis-NIR spectroscopy and align with the transformation of the PPy structure from an irregular to a sheet-like structure (Scheme 1c), particularly the ratio in C−C ring deformation and in C−H deformation. The increase in the bipolaron/polaron ratio is associated with band gap reduction (drop from 3.21 to 1.74 eV), indicating an enhanced degree of oxidation for PPy as the APS/Py ratio increased. Although the bipolaron/polaron ratio dropped when the APS/Py ratio increased, those ratios showed a low energy gap and low resistance. It was assumed that the sheet-like structure, which occurred in cooperation with SDS, might be a factor that helps

https://doi.org/10.1021/acsomega.3c06511
ACS Omega 2023, 8, 48946−48957

Scheme 3. Schematic Diagram of PPy Polymerization

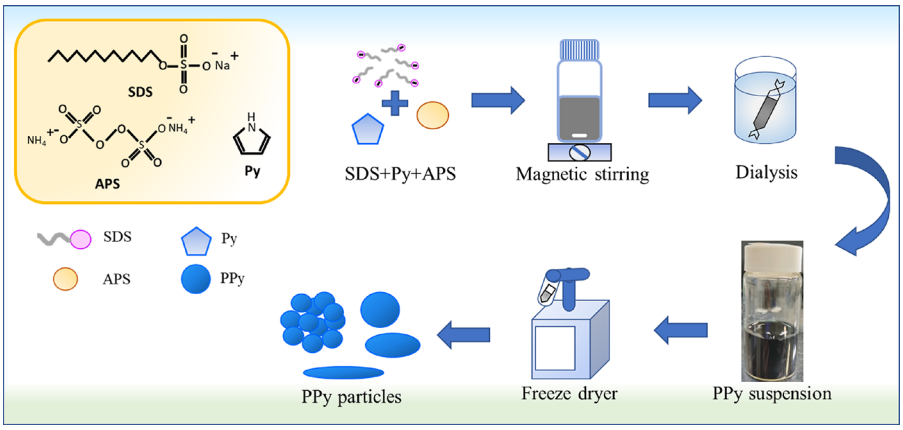

to maintain the band gap properties of PPy compared to no surfactant.[56,61]

The results of varying the Py concentrations, SDS concentration, and APS/Py during the synthesis of PPy demonstrate that different concentrations of the components lead to distinct oxidative states of PPy, as observed from the shift in the UV−vis-NIR absorbance peaks and the appearance of bipolaron and polaron structures in the Raman spectra. Specifically, an increase in the Py concentration and the APS/Py ratio resulted in high oxidative states in PPy. The increase in the average size of PPy correlated with a reduction in its optical band gap, possibly because of the enhancement of its conductivity resulting from its large surface area. This correlation was confirmed by the decrease in the resistance of PPy and transformation of its morphology from a combination of particles and sheet-like structures to purely sheet-like structures with increasing Py concentrations (Scheme 1). At Py concentrations in the range from 0.10 to 0.30 M, the bipolaron/polaron ratio of C−C ring stretching and C−H deformation was observed to shift toward a bipolaron state in PPy, whereas the ratio remained unchanged in PPy*. These results suggest that combining SDS with an appropriate amount of Py would effectively promote the conductivity of PPy. Additionally, SDS promoted the bipolaron/polaron ratio of C−H deformation and affected the physical morphology of PPy. The observed variations in the morphology and size of PPy could be partly attributed to the different C−H bond structures formed when an SDS template was used during the polymerization process.

3. CONCLUSIONS

This work aims to investigate the effects of SDS on the chemical polymerization of PPy and to explore the correlations between its properties. It was found that SDS functioned as a template for Py polymerization and influenced the physical, electrical, and chemical properties of PPy. Py was polymerized within the micellar structure of an SDS template. Their morphologies transformed from random forms to sheet-like forms and enlarged the size structure when the Py concentration and APS/Py ratio increased using 0.01 M SDS. On the contrary to PPy* (PPy synthesized in the absence of SDS), only a sphere-like form was found. SDS assists PPy in the enhancement of the electrical properties. Optical band gap and conductivity increased when the Py concentration and the APS/Py ratio increased as compared to PPy*. The Raman spectra showed that SDS promoted a chemical change in PPy, as shown in the ratio between bipolarons and polarons, particularly in C−C ring stretching and C−H deformation. It was found that the ratio increased as the Py concentration and the APS/Py ratio increased but the corresponding ratio for PPy* remained almost unchanged as the Py concentration increased. However, SDS concentrations ranging from 0.01 to 0.30 M had no significant effect on the optical band gap or average size of the PPy sheets while using 0.04 M Py and an APS/Py ratio of 1. This work revealed a correlation among the average size, morphology, and electrical characteristics. The increase in average size was related to a decrease in band gap and resistance. The ratio of C−H deformation in PPy was larger than in PPy* indicating that SDS increased C−H deformation in PPy, which changed its physical shape and then influenced its electrical characteristics via the correlation between size and band gap, or resistance.

Consequently, SDS was crucial in changing the shape of PPy, enhancing the conductivity, and changing the ratio of bipolarons to polarons in PPy. The proportion of each material (Py monomer, SDS, and APS) was also critical in defining its characteristics. This study highlights the correlation between the bipolaron/polaron ratio of PPy relating to its chemical structure, electronic structure, and morphology, providing a deeper understanding of their characteristics that can be utilized to design materials with specific properties.

4. EXPERIMENTAL SECTION

4.1. Materials. The Py used in the experiments (98% reagent grade, Sigma-Aldrich Co., LLC, St. Louis, Missouri, USA) was refrigerated before its use. SDS and APS were provided by Wako Pure Chemical Industries Ltd., Osaka, Japan. All aqueous solutions were prepared using ultrapure water (18.2 MΩ resistance, Direct-Q 3 UV, Merck Millipore, Osaka, Japan). Indium tin oxide (ITO) glass electrodes were purchased from BAS Inc., Tokyo, Japan. Silver paint (resistance ≤1 Ω) was purchased from Polycalm, Japan. All the electrochemical tests were conducted using an automatic polarization system (HZ-7000, Hokuto Denko Corporation, Tokyo, Japan).

4.2. PPy Synthesis. Chemical polymerization was used to synthesize the PPy samples. Py was added to the SDS solution first, and the mixture was agitated for 2 h at 25 °C ambient temperature. Following that, an APS solution was gradually added to the mixture. By altering the APS/Py ratio as well as the Py and SDS concentrations, we investigated the impact of the Py, SDS, and APS concentrations on polymer synthesis.

https://doi.org/10.1021/acsomega.3c06511
ACS Omega 2023, 8, 48946−48957

The mixture was stirred for 24 h at room temperature (25 °C) (Scheme 3), and a dark-blue PPy powder suspension was obtained. It was dialyzed in ultrapure water to remove any unreacted monomer as well as SDS, and APS from the synthesized PPy. PPy was obtained as a slurry, freeze-dried, and stored in a desiccator until its use. To study the effect of Py on PPy, the Py concentration (APS/Py ratio of 1.00) was varied while maintaining the SDS concentration constant at 0.10 M. To study the effect of SDS on PPy, the Py and APS concentrations were set at 0.04 M while varying the SDS concentrations. To study the effect of APS on PPy, the APS and Py molar ratio (APS/Py) was varied from 0.05 to 3.50 while the concentration of SDS was 0.10 and the Py concentration was 0.04 M (Scheme 3).

4.3. Sample Characterizations. *4.3.1. Particle Size Distribution and Zeta Potential.* PPy was suspended in ultrapure water (0.1−0.2 mg/mL). The suspension was tested for particle size distribution and zeta potential using the DLS apparatus ZEN5600 Zetasizer manufactured by Malvern Instruments Ltd., Worcestershire, United Kingdom.

4.3.2. SEM. The dried PPy powder was obtained from the freeze-dryer and stored in a desiccator until analysis. The morphology of dried PPy powder was analyzed by scanning electron microscopy (JCM-7000, JEOL Ltd., Japan)

4.3.3. Ultraviolet/Visible/Near Infrared (UV−vis-NIR) Absorbance and Optical Band Gap. The optical properties of PPy were analyzed by using UV−vis-NIR spectroscopy (UV1800, Shimadzu, Japan). PPy was diluted and suspended in ultrapure water (0.1−0.2 mg/mL) in a quartz cuvette with a 10 mm path length. The light absorbance of the samples was monitored and analyzed based on the optical band gap determined using Tauc's correlation, as shown in eq 1.

$$(\alpha h\nu)^{1/n} = \alpha_0(h\nu - E_g) \tag{1}$$

where α is the absorption coefficient ($2.302 \times A/d$), d is the cell thickness (1 cm), A is the light absorbance, $h\nu$ is the photon energy (eV), h is the Planck's constant (6.6261×10^{-34} J·s), and ν is the photon frequency with $\nu = C/\lambda$ where C = speed of light (2.998×10^8 m/s), λ is the wavelength (nm), photon energy (eV) is $1240/\lambda$, E_g is the optical band gap (eV), α_o is a constant band-tailing parameter, and n is the power factor ($n = 2$ for an indirect transition band gap).[9,62] The plot of $(\alpha h\nu)^{1/n}$ versus photon energy ($h\nu$) will be a straight line within a specific region. The optical band gap was obtained by extrapolating the straight-line intercept along the ($h\nu$) axis.

4.3.4. Electrical Conductivity Analysis. The PPy powder was cast into pellets (0.005 g/cm^2) by using a hand press and sandwiched between two ITO glass electrodes (Scheme S1). The distance between the electrodes and the thickness of the pellet were maintained at their initial values by using 0.8 mm-thick silicone rubber. The resistance of PPy was monitored using a two-point probe measurement technique in the LSV mode with a potential window between −1.8 and +1.8 V, scanned at a rate of 50 mV/s with 10 points recorded per scan. The data were monitored and recorded using an automatic polarization system (HZ-7000, Hokuto Denko Corporation, Tokyo, Japan), connected to a personal computer. The resistance values were measured and averaged for three different electrodes using fresh PPy. Each resistance value was obtained from the slope of an I/V plot based on Ohm's law. The conductivity of PPy was determined using the correlations shown in eqs 2 and 3.

$$\rho = \frac{RA}{L} \tag{2}$$

$$\sigma = \frac{1}{\rho} \tag{3}$$

where R is the resistance of PPy (Ω), ρ is the resistivity of PPy (Ω·m), L is the thickness of silicon rubber (8.00×10^{-4} m), A is the area of the sample (1.96×10^{-5} m^2), and σ is the electrical conductivity (S/m).

4.3.5. Raman Spectroscopy. The Raman spectra of PPy were investigated from a Raman spectrometer (HR-800, Horiba Ltd., Kyoto, Japan) with a laser excitation wavelength of 532 nm. The peak intensities (Is) of the bipolarons and polarons in PPy (Table S1) were analyzed using OriginPro software (OriginPro, Version 2023. OriginLab Corporation, Northampton, Massachusetts, USA.). The ratio of the peak intensity of the bipolarons to that of the polarons was then determined.

■ ASSOCIATED CONTENT

Supporting Information

AUTHOR INFORMATION The Supporting Information is available free of charge at https://pubs.acs.org/doi/10.1021/acsomega.3c06511.

Schematic of the resistance measurement system; resistance results comparing between PPy with and without SDS; SEM images (×5000) displaying the surface morphologies of the PPy samples; absorbance from UV−vis-NIR spectroscopy; Tauc plots of the PPy samples; Raman spectra: PPy and the SDS solution with marks from the CH_2 group and PPy synthesized with no SDS; peak attribution reference of Raman spectra at different excitation levels; and morphology of PPy from SEM, zeta potential, and conductivity (PDF)

■ AUTHOR INFORMATION

Corresponding Authors

Hiroshi Umakoshi − *Division of Chemical Engineering, Graduate School of Engineering Science, Osaka University, Toyonaka 560-8531 Osaka, Japan;* orcid.org/0000-0002-9241-853X; Phone: +81-6-6850-6287; Email: umakoshi.hiroshi.es@osaka-u.ac.jp; Fax: +81-6-6850-6286

Thaneeya Samwang − *Division of Chemical Engineering, Graduate School of Engineering Science, Osaka University, Toyonaka 560-8531 Osaka, Japan; Department of Chemical Engineering, Faculty of Engineering, Mahidol University, Nakhon Pathom 73170, Thailand*; Phone: +81-6-6850-6287; Email: thaneeya.sam@mahidol.edu; Fax: +81-6-6850-6286

Authors

Nozomi Morishita Watanabe − *Division of Chemical Engineering, Graduate School of Engineering Science, Osaka University, Toyonaka 560-8531 Osaka, Japan*

Yukihiro Okamoto − *Division of Chemical Engineering, Graduate School of Engineering Science, Osaka University, Toyonaka 560-8531 Osaka, Japan*

Sira Srinives − *Department of Chemical Engineering, Faculty of Engineering, Mahidol University, Nakhon Pathom 73170, Thailand;* orcid.org/0000-0002-7890-1103

Complete contact information is available at:

https://doi.org/10.1021/acsomega.3c06511
ACS Omega 2023, 8, 48946−48957

https://pubs.acs.org/10.1021/acsomega.3c06511

Author Contributions

The manuscript was written using contributions made by T.S., S.S., N.M.W., and Y.O. H.U. and S.S. supervised the conduct of study. All of the authors reviewed and carefully revised the draft manuscript. All of them have approved the final version of the manuscript.

Notes

The authors declare no competing financial interest.

■ ACKNOWLEDGMENTS

This work was primarily supported by the Japan Society for the Promotion of Science KAKENHI Grant-in-Aids for Scientific Research (A) (21H04628) and the Royal Thai Government Scholarship program. The authors gratefully thank Prof. Dr. Norikazu Nishiyama for SEM analysis.

■ REFERENCES

(1) Xiaoqiang, L.; Qian, S.; Yan, K.; Yanan, Z.; Zengyuan, P.; Yang, J.; Mengjuan, L.; Chronakis, I. S. Self-Powered Humidity Sensor Based on Polypyrrole Modified Melamine Aerogel. *Mater. Lett.* **2020**, *277*, No. 128281.

(2) Miao, J.; Chen, Y.; Li, Y.; Cheng, J.; Wu, Q.; Ng, K. W.; Cheng, X.; Chen, R.; Cheng, C.; Tang, Z. Proton Conducting Polyoxometalate/Polypyrrole Films and Their Humidity Sensing Performance. *ACS Appl. Nano Mater.* **2018**, *1* (2), 564−571.

(3) De Aguiar, M. F.; Leal, A. N. R.; De Melo, C. P.; Alves, K. G. B. Polypyrrole-Coated Electrospun Polystyrene Films as Humidity Sensors. *Talanta* **2021**, *234*, No. 122636.

(4) Miah, M. R.; Yang, M.; Khandaker, S.; Bashar, M. M.; Alsukaibi, A. K. D.; Hassan, H. M. A.; Znad, H.; Awual, Md. R. Polypyrrole-Based Sensors for Volatile Organic Compounds (VOCs) Sensing and Capturing: A Comprehensive Review. *Sens. Actuators Phys.* **2022**, *347*, No. 113933.

(5) Qi, R.; Lin, X.; Dai, J.; Zhao, H.; Liu, S.; Fei, T.; Zhang, T. Humidity Sensors Based on MCM-41/Polypyrrole Hybrid Film via in-Situ Polymerization. *Sens. Actuators B Chem.* **2018**, *277*, 584−590.

(6) Zang, L.; Liu, Q.; Qiu, J.; Yang, C.; Wei, C.; Liu, C.; Lao, L. Design and Fabrication of an All-Solid-State Polymer Supercapacitor with Highly Mechanical Flexibility Based on Polypyrrole Hydrogel. *ACS Appl. Mater. Interfaces* **2017**, *9* (39), 33941−33947.

(7) Han, X.; Xiao, G.; Wang, Y.; Chen, X.; Duan, G.; Wu, Y.; Gong, X.; Wang, H. Design and Fabrication of Conductive Polymer Hydrogels and Their Applications in Flexible Supercapacitors. *J. Mater. Chem. A* **2020**, *8* (44), 23059−23095.

(8) Shabeeba, A.; Rajan, L.; Sidheekha, M. P.; Thayyil, M. S.; Ismail, Y. A. Polypyrrole/Hydrogel Hybrid Films as Multi Sensing Supercapacitor Electrodes. *J. Energy Storage* **2022**, *55*, No. 105724.

(9) Lin, Q.; Yang, Y.; Ma, Y.; Zhang, R.; Wang, J.; Chen, X.; Shao, Z. Bandgap Engineered Polypyrrole−Polydopamine Hybrid with Intrinsic Raman and Photoacoustic Imaging Contrasts. *Nano Lett.* **2018**, *18* (12), 7485−7493.

(10) George, P. M.; Lyckman, A. W.; LaVan, D. A.; Hegde, A.; Leung, Y.; Avasare, R.; Testa, C.; Alexander, P. M.; Langer, R.; Sur, M. Fabrication and Biocompatibility of Polypyrrole Implants Suitable for Neural Prosthetics. *Biomaterials* **2005**, *26* (17), 3511−3519.

(11) Veisi, H.; Varshosaz, J.; Rostami, M.; Mirian, M. Thermosensitive TMPO-Oxidized Lignocellulose/Cationic Agarose Hydrogel Loaded with Deferasirox Nanoparticles for Photothermal Therapy in Melanoma. *Int. J. Biol. Macromol.* **2023**, *238*, No. 124126.

(12) Ramanaviciene, A.; Kausaite, A.; Tautkus, S.; Ramanavicius, A. Biocompatibility of Polypyrrole Particles: An in-Vivo Study in Mice. *J. Pharm. Pharmacol.* **2010**, *59* (2), 311−315.

(13) Ashery, A.; Salem, M. A.; Farag, A. A. M. Optical and Electrical Performance of Ploypyrrol Thin Films and Its Hybrid Junction Applications. *Optik* **2018**, *172*, 302−310.

(14) Salzner, U.; Lagowski, J. B.; Pickup, P. G.; Poirier, R. A. Comparison of Geometries and Electronic Structures of Polyacetylene, Polyborole, Polycyclopentadiene, Polypyrrole, Polyfuran, Polysilole, Polyphosphole, Polythiophene, Polyselenophene and Polytellurophene. *Synth. Met.* **1998**, *96* (3), 177−189.

(15) Iurchenkova, A. A.; Kallio, T.; Fedorovskaya, E. O. Relationships between Polypyrrole Synthesis Conditions, Its Morphology and Electronic Structure with Supercapacitor Properties Measured in Electrolytes with Different Ions and pH Values. *Electrochim. Acta* **2021**, *391*, No. 138892.

(16) Atta, A.; Negm, H.; Abdeltwab, E.; Rabia, M.; Abdelhamied, M. M. Facile Fabrication of Polypyrrole/NiOx Core-Shell Nanocomposites for Hydrogen Production from Wastewater. *Polym. Adv. Technol.* **2023**, *34* (5), 1633−1641.

(17) Bayat, M.; Izadan, H.; Santiago, S.; Estrany, F.; Dinari, M.; Semnani, D.; Alemán, C.; Guirado, G. Study on the Electrochromic Properties of Polypyrrole Layers Doped with Different Dye Molecules. *J. Electroanal. Chem.* **2021**, *886*, No. 115113.

(18) Yang, Y.; Jin, Y.; He, H.; Wang, Q.; Tu, Y.; Lu, H.; Ye, Z. Dopant-Induced Shape Evolution of Colloidal Nanocrystals: The Case of Zinc Oxide. *J. Am. Chem. Soc.* **2010**, *132* (38), 13381−13394.

(19) Choudhury, B.; Choudhury, A. Dopant Induced Changes in Structural and Optical Properties of Cr3+ Doped TiO2 Nanoparticles. *Mater. Chem. Phys.* **2012**, *132* (2−3), 1112−1118.

(20) Chitte, H. K.; Shinde, G. N.; Bhat, N. V.; Walunj, V. E. Synthesis of Polypyrrole Using Ferric Chloride (FeCl<-Sub>3</Sub>) as Oxidant Together with Some Dopants for Use in Gas Sensors. *J. Sens. Technol.* **2011**, *01* (02), 47−56.

(21) Thompson, B. C.; Moulton, S. E.; Richardson, R. T.; Wallace, G. G. Effect of the Dopant Anion in Polypyrrole on Nerve Growth and Release of a Neurotrophic Protein. *Biomaterials* **2011**, *32* (15), 3822−3831.

(22) Wang, Y.; Song, R.; Li, L.; Fu, R.; Liu, Z.; Li, B. High Crystalline Quality Conductive Polypyrrole Film Prepared by Interface Chemical Oxidation Polymerization Method. *Appl. Sci.* **2022**, *12* (1), 58.

(23) Hou, Y.; Zhang, L.; Chen, L. Y.; Liu, P.; Hirata, A.; Chen, M. W. Raman Characterization of Pseudocapacitive Behavior of Polypyrrole on Nanoporous Gold. *Phys. Chem. Chem. Phys.* **2014**, *16* (8), 3523.

(24) Zhou, M.; Pagels, M.; Geschke, B.; Heinze, J. Electropolymerization of Pyrrole and Electrochemical Study of Polypyrrole. 5. Controlled Electrochemical Synthesis and Solid-State Transition of Well-Defined Polypyrrole Variants. *J. Phys. Chem. B* **2002**, *106* (39), 10065−10073.

(25) Gupta, S. Hydrogen Bubble-Assisted Syntheses of Polypyrrole Micro/nanostructures Using Electrochemistry: Structural and Physical Property Characterization. *J. Raman Spectrosc.* **2008**, *39* (10), 1343−1355.

(26) Appel, G.; Böhme, O.; Mikalo, R.; Schmeißer, D. The polaron and bipolaron Contributions to the Electronic Structure of Polypyrrole Films. *Chem. Phys. Lett.* **1999**, *313* (3−4), 411−415.

(27) Brédas, J. L.; Scott, J. C.; Yakushi, K.; Street, G. B. Polarons and bipolarons in Polypyrrole: Evolution of the Band Structure and Optical Spectrum upon Doing. *Phys. Rev. B* **1984**, *30* (2), 1023−1025.

(28) Santos, M. J. L.; Brolo, A. G.; Girotto, E. M. Study of polaron and bipolaron States in Polypyrrole by in Situ Raman Spectroelectrochemistry. *Electrochim. Acta* **2007**, *52* (20), 6141−6145.

(29) Pang, S.-K. Comprehensive Study of Polymerization of Pyrrole: A Theoretical Approach. *J. Electroanal. Chem.* **2020**, *859*, No. 113886.

(30) Šetka, M.; Calavia, R.; Vojku°vka, L.; Llobet, E.; Drbohlavová, J.; Vallejos, S. Raman and XPS Studies of Ammonia Sensitive Polypyrrole Nanorods and Nanoparticles. *Sci. Rep.* **2019**, *9* (1), 8465.

(31) Bober, P.; Li, Y.; Acharya, U.; Panthi, Y.; Pfleger, J.; Humpolíček, P.; Trchová, M.; Stejskal, J. Acid Blue Dyes in Polypyrrole Synthesis: The Control of Polymer Morphology at Nanoscale in the Promotion of High Conductivity and the Reduction of Cytotoxicity. *Synth. Met.* **2018**, *237*, 40−49.

(32) Ishpal; Kaur, A. Spectroscopic and Electrical Sensing Mechanism in Oxidant-Mediated Polypyrrole Nanofibers/Nanoparticles for Ammonia Gas. *J. Nanoparticle Res.* **2013**, *15* (5), 1637.
(33) Trchová, M.; Stejskal, J. Resonance Raman Spectroscopy of Conducting Polypyrrole Nanotubes: Disordered Surface versus Ordered Body. *J. Phys. Chem. A* **2018**, *122* (48), 9298−9306.
(34) Zhou, Z.; Shao, Y.; Gao, X.; Liu, Z.; Zhang, Q. Structural Regulation of Polypyrrole Nanospheres Guided by Hydrophobic Chain Length of Surfactants. *J. Mater. Sci.* **2019**, *54* (23), 14309−14319.
(35) Fan, X.; Yang, Z.; He, N. Hierarchical Nanostructured Polypyrrole/Graphene Composites as Supercapacitor Electrode. *RSC Adv.* **2015**, *5* (20), 15096−15102.
(36) Deljoo Kojabad, Z.; Shojaosadati, S. A. Chemical Synthesis of Polypyrrole nanostructures: Optimization and Applications for Neural Microelectrodes. *Mater. Des.* **2016**, *96*, 378−384.
(37) Mao, J.; Li, C.; Park, H. J.; Rouabhia, M.; Zhang, Z. Conductive Polymer Waving in Liquid Nitrogen. *ACS Nano* **2017**, *11* (10), 10409−10416.
(38) Roohi, Z.; Mighri, F.; Zhang, Z. A Simple Trick to Increase the Areal Specific Capacity of Polypyrrole Membrane: The Superposition Effect of Methyl Orange and Acid Treatment. *Polymers* **2022**, *14* (21), 4693.
(39) Qin, G.; Qiu, J. Ordered Polypyrrole Nanorings with Near-Infrared Spectrum Absorption and Photothermal Conversion Performance. *Chem. Eng. J.* **2019**, *359*, 652−661.
(40) Yang, X.; Lin, Z.; Zheng, J.; Huang, Y.; Chen, B.; Mai, Y.; Feng, X. Facile Template-Free Synthesis of Vertically Aligned Polypyrrole Nanosheets on Nickel Foams for Flexible All-Solid-State Asymmetric Supercapacitors. *Nanoscale* **2016**, *8* (16), 8650−8657.
(41) Xie, Y.; Xu, J.; Jin, H.; Yi, Y.; Shen, Y.; Zhang, X.; Liu, X.; Sun, Y.; Shi, W.; He, Y.; Ge, D. Polypyrrole Nanosheets Prepared by Rapid In Situ Polymerization for NIR-II Photoacoustic-Guided Photothermal Tumor Therapy. *Coatings* **2023**, *13* (6), 1037.
(42) Guan, H.; Ding, T.; Zhou, W.; Wang, Z.; Zhang, J.; Cai, K. Hexagonal Polypyrrole Nanosheets from Interface Driven Heterogeneous Hybridization and Self-Assembly for Photothermal Cancer Treatment. *Chem. Commun.* **2019**, *55* (30), 4359−4362.
(43) Zhang, X.; Zhang, J.; Song, W.; Liu, Z. Controllable Synthesis of Conducting Polypyrrole nanostructures. *J. Phys. Chem. B* **2006**, *110* (3), 1158−1165.
(44) Hazarika, J.; Kumar, A. Controllable Synthesis and Characterization of Polypyrrole Nanoparticles in Sodium Dodecylsulphate (SDS) Micellar Solutions. *Synth. Met.* **2013**, *175*, 155−162.
(45) Direksilp, C.; Sirivat, A. Synthesis and Characterization of Hollow-Sphered Poly(N-Methyaniline) for Enhanced Electrical Conductivity Based on the Anionic Surfactant Templates and Doping. *Polymers* **2020**, *12* (5), 1023.
(46) Gangopadhyay, R. Peering into Polypyrrole-SDS Nanodispersions: Rheological View. *J. Appl. Polym. Sci.* **2013**, *128*, 1398−1408.
(47) Xing, S.; Zhao, G. Morphology, Structure, and Conductivity of Polypyrrole Prepared in the Presence of Mixed Surfactants in Aqueous Solutions. *J. Appl. Polym. Sci.* **2007**, *104* (3), 1987−1996.
(48) Hoshina, Y.; Zaragoza-Contreras, E. A.; Farnood, R.; Kobayashi, T. Nanosized Polypyrrole Affected by Surfactant Agitation for Emulsion Polymerization. *Polym. Bull.* **2012**, *68* (6), 1689−1705.
(49) Morávková, Z.; Taboubi, O.; Minisy, I. M.; Bober, P. The Evolution of the Molecular Structure of Polypyrrole during Chemical Polymerization. *Synth. Met.* **2021**, *271*, No. 116608.
(50) Kausaite-Minkstimiene, A.; Mazeiko, V.; Ramanaviciene, A.; Ramanavicius, A. Evaluation of Chemical Synthesis of Polypyrrole Particles. *Colloids Surf. Physicochem. Eng. Asp.* **2015**, *483*, 224−231.
(51) Yun, S.-R.; Kim, G.-O.; Lee, C. W.; Jo, N.-J.; Kang, Y.; Ryu, K.-S. Synthesis and Control of the Shell Thickness of Polyaniline and Polypyrrole Half Hollow Spheres Using the Polystyrene Cores. *J. Nanomater.* **2012**, *2012*, 1−9.
(52) Paúrová, M.; Šeděnková, I.; Hromádková, J.; Babič, M. Polypyrrole Nanoparticles: Control of the Size and Morphology. *J. Polym. Res.* **2020**, *27* (12), 366.
(53) Vigmond, S. J.; Ghaemmaghami, V.; Thompson, M. Raman and Resonance-Raman Spectra of Polypyrrole with Application to Sensor − Gas Probe Interactions. *Can. J. Chem.* **1995**, *73* (10), 1711−1718.
(54) Scott, J. C.; Bredas, J. L.; Yakushi, K.; Pfluger, P.; Street, G. B. The Evidence for bipolarons in Pyrrole Polymers. *Synth. Met.* **1984**, *9* (2), 165−172.
(55) Abdullah, B. J. Size Effect of Band Gap in Semiconductor Nanocrystals and nanostructures from Density Functional Theory within HSE06. *Mater. Sci. Semicond. Process.* **2022**, *137*, No. 106214.
(56) Pang, A. L.; Arsad, A.; Rezaei Ardani, M.; Ismail, N. E.; Julkapli, N. M.; Ahmadipour, M. Exploring the Impact of Oxidant Ratio on Polypyrrole Properties: Electrical, Optical, and Adsorption Behaviour. *Inorg. Chem. Commun.* **2023**, *155*, No. 111052.
(57) Singh, D. V. K. BAND GAP AND RESISTIVITY MEASUREMENTS OF SEMICONDUCTOR MATERIALS FOR THIN FILMS. 2017, *4*.
(58) Nah, J.; Perkins, F. K.; Lock, E. H.; Nath, A.; Boyd, A.; Myers-Ward, R. L.; Gaskill, D. K.; Osofsky, M.; Rao, M. V. Electrical and Low Frequency Noise Characterization of Graphene Chemical Sensor Devices Having Different Geometries. *Sensors* **2022**, *22* (3), 1183.
(59) Poblette-Almazán, L. D.; Moreno-Saavedra, H.; Hernández-Tenorio, C.; Borja-Salín, M. A. Electrical Resistance of Electrochemical Synthesized Polypyrrole in the Presence of Sodium Dodecyl Sulfate Surfactant. *MRS Adv.* **2022**, *7* (34), 1150−1153.
(60) Jeeju, P. P.; Varma, S. J.; Francis Xavier, P. A.; Sajimol, A. M.; Jayalekshmi, S. Novel Polypyrrole Films with Excellent Crystallinity and Good Thermal Stability. *Mater. Chem. Phys.* **2012**, *134* (2−3), 803−808.
(61) Deng, J.; Wang, X.; Guo, J.; Liu, P. Effect of the Oxidant/Monomer Ratio and the Washing Post-Treatment on Electrochemical Properties of Conductive Polymers. *Ind. Eng. Chem. Res.* **2014**, *53* (35), 13680−13689.
(62) Lertthanaphol, N.; Prawiset, N.; Soontornapaluk, P.; Kitjanukit, N.; Neamsung, W.; Pienutsa, N.; Chusri, K.; Sornsuchat, T.; Chanthara, P.; Phadungbut, P.; Seeharaj, P.; Kim-Lohsoontorn, P.; Srinives, S. Soft Template-Assisted Copper-Doped Sodium Dititanate Nanosheet/Graphene Oxide Heterostructure for Photoreduction of Carbon Dioxide to Liquid Fuels. *RSC Adv.* **2022**, *12* (37), 24362−24373.

https://doi.org/10.1021/acsomega.3c06511
ACS Omega 2023, 8, 48946−48957